Renewable and Sustainable Energy Reviews 140 (2021) 110731

Contents lists available at ScienceDirect

Renewable and Sustainable Energy Reviews

journal homepage: http://www.elsevier.com/locate/rser

# Combined capacity and operation optimisation of lithium-ion battery energy storage working with a combined heat and power system

Dacheng Li *, Songshan Guo, Wei He, Marcus King, Jihong Wang

*School of Engineering, University of Warwick, Coventry, CV4 7AL, UK*

ARTICLE INFO

*Keywords:*
Combined planning
CHP
Lithium-ion battery storage system
Capacity
Strategy
Economy
Optimisation

ABSTRACT

Combined Heat and Power (CHP) systems are considered as a transitional solution towards zero carbon emissions in the next couple of decades. The current CHP systems are mainly controlled by thermal led strategy, that is, the electrical power generation depends on the thermal energy demand. The mismatch between the power generation and load demand leads to the deficient energy utilisation and economic loss. An innovative combined planning method is proposed in the paper to improve the economic gains of the CHP systems by integrating the lithium-ion battery storage system (LBSS). The paper focuses on the simultaneous optimisation of storage capacity design and operation strategy formulation of the LBSS subject to the variations of the load and power generation from CHP with consideration of LBSS degradation and cost, and Time-of-Use pricing structures. The new strategy is implemented and tested using the University of Warwick campus CHP system combined with the LBSS facilities. The results show that the method could improve the economic performance of CHP systems. The developed method is applicable to any CHP systems optimisation with integrated LBSS.

## 1. Introduction

Combined Heat and Power (CHP) technology allows for the production of electricity and heat simultaneously from a single fuel source [1,2]. By recovering waste heat from the engine exhaust, CHP systems achieve high working efficiencies (typically>80%) and reduce greenhouse gas emissions by up to 30% during operation [3,4]. As a mature and effective approach to reduce greenhouse gas emission, the UK has now installed over 21 GW-thermal and 6 GW-electric (~7% of total power generation) CHP systems and reduced annual carbon emissions by 10.33 Mton (~15% the national total carbon emission in 2018) [5]. The global CHP market is poised to grow by 124.76 GW during 2019–2023 [6].

CHP systems usually run in a "thermally-lead" mode in residential applications where heating supply is matched to the heating load [7–9]. As a result, there is often a mismatch between the generation and demand for electricity. If the production of electricity exceeds the user requirement, the extra electrical power generation is fed into the grid; conversely, when there is a lack of electrical generation, the residual load has to be drawn from the grid. Because of the low price of electricity exported to the grid from the local energy system (only in the case that the exporting license is issued otherwise, it is free power fed to grid), CHP systems usually cannot gain revenue by doing so, increasing the cost of the system. In this context, electrical energy storage technologies could open up an opportunity to reduce energy bills by improving power utilisation locally and mitigate otherwise necessary network upgrades [10]. Moreover, electricity storage could also enable the integrated system to gain additional economic benefits using the Time-of-Use (ToU) pricing structures [11].

Lithium-ion Battery (LIB) is a promising electrical storage technology because of its high energy density and Coulombic efficiency [11–13]. Investigations have shown that the integration of a Lithium-ion Battery Storage System (LBSS) with CHP systems can provide operational flexibility and improve the self-sufficiency rate [14,15]. Nevertheless, the high initial investment of battery storage has limited their utilisation to present for improving the integrated energy system economy and reducing carbon emissions [16,17]. However, recently the manufacturing cost of these batteries has decreased substantially, potentially enabling LBSS to become economically viable by capturing grid revenue under the ToU electricity tariff [18–21].

To minimise the cost of battery storage-integrated energy systems, Kerdphol et al. [22] proposed a particle swarm optimisation based method to optimise the size of a Battery Energy Storage System (BESS) in

* Corresponding author.
*E-mail addresses:* Dacheng.Li@warwick.ac.uk (D. Li), S.Guo.5@warwick.ac.uk (S. Guo), Wei.He.2@warwick.ac.uk (W. He), Marcus.King@warwick.ac.uk (M. King), Jihong.Wang@warwick.ac.uk (J. Wang).

https://doi.org/10.1016/j.rser.2021.110731
Received 27 March 2020; Received in revised form 28 November 2020; Accepted 11 January 2021
Available online 23 January 2021

**List of abbreviations**

| | |
|---|---|
| BESS | Battery Energy Storage System |
| BBO | Biogeography-Based Optimisation |
| CHP | Combined Heat and Power |
| DOD | Depth Of Discharge |
| HSI | Habitat Suitability Index |
| LIB | Lithium-ion Battery |
| LBSS | Lithium-ion Battery Storage System |
| NOB | Number of Battery |
| SOC | State Of Charge |
| ToU | Time-of-Use |
| UoW | University of Warwick |

*List of nomenclature*

| | |
|---|---|
| $A$, $B$ | parameters of investment model of LBSS |
| $a$, $b$ | parameters of model of SOC reduction rate during the standby process |
| $C_{daily}$ | daily capital cost of LBSS (GBP) |
| $C_{elec}$ | grid electricity price (GBP/kWh) |
| $C_{invest}$ | investment cost (GBP/kWh) |
| $C_{re}$ | reactive power charge fee (GBP/kWh) |
| $C_{ToU}$ | Time-of-Use price (GBP/kWh) |
| $Cl$ | cycle life |
| $D$ | dimension |
| $E_{CHP}$ | CHP generation output (kWh) |
| $E_{load}$ | electrical load demand (kWh) |
| $F$ | flag |
| $Lt$ | calendar lifetime of the battery (day) |
| $n$ | number of the control segment |
| $P_{CHP}$ | CHP power output (kW) |
| $P_{CHPS}$ | charge power input by the CHP system (kW) |
| $P_{discharge}$ | battery discharge power (kW) |
| $P_{grid}$ | charge power input by the grid (kW) |
| $P_{inverter}$ | power of the inverter (kW) |
| $Q_{battery}$ | capacity of the battery (kWh) |
| $SOC_{loss}$ | SOC reduction rate (%/h) |
| $t_{charge}$ | battery charge time (h) |
| $t_{CHPS}$ | CHP charge time (h) |
| $t_{discharge}$ | battery discharge time (h) |
| $t_s$ | time interval in the control segment (h) |

*Greek symbols*

| | |
|---|---|
| $\eta$ | efficiency of the LBSS (%) |
| $\theta$ | value of SOC (%) |

*Subscripts*

| | |
|---|---|
| battery | battery |
| charge | charge |
| CHPS | CHP system |
| daily | daily |
| discharge | discharge |
| elec | electricity |
| grid | grid |
| inverter | inverter |
| load | load |
| loss | loss |
| rated | rated |
| re | reactive |
| residual | residual |

a microgrid. The economic performance of a polysulfide–bromine BESS and a vanadium redox BESS was studied and compared to find a low investment cost solution. Liu et al. [23] presented an optimisation strategy for sizing power sources and electricity storage. The characteristics of LIB and lead-acid battery were considered in optimising procedure to form a hybrid energy storage system to improve the economic benefit. An investigation also proceeded to control the cycling of BESS integrated in a grid-supporting PV system for minimising the power injection to the grid [24]. Dynamic programming was used in Ref. [24] to obtain an optimal operating strategy of the batteries under different sell-back policies. Wu et al. [25] proposed a stochastic approach to minimise electricity cost of smart home microgrid by integrating plug-in electric vehicle (PEV) battery storage. Optimal power allocation among the PEV battery, home power demand, and utility grid was conducted under various operating modes of PEV. Additionally, Zhang et al. [26] optimised the manufacturing schedules and energy flow of a grid-connected factory with an onsite PV and battery system to reduce the electricity cost under different ToU rates.

These prior studies mainly focused on either capacity optimisation or optimal control of the battery storage system to maximise the system economics. However, the lifetime cash flow of battery storage integrated CHP system is inherently complex. An installation of LBSS leads to an increase in system capital expenditure; real-time operation of the battery system under varying user-load patterns and ToU rates determines the system operating expenses (including revenues), and the LBSS system lifetime [27–30]. All these factors are coupled and interactively affect the economic viability of using LBSS in CHP systems.

Therefore, to further reduce the cost of battery storage integrated CHP systems, a new planning method that combines the capacity design and operational strategy optimisation is proposed in this study. To our knowledge, this is the first study regarding combined planning of LBSS for CHP systems to have a lower cost to meet seasonally varying user demand patterns, compared to current CHP systems. To show the method and cost reduction potential of CHP systems, the remainder of this paper is organised as follows. Section 2 discusses the ToU pricing structure and analyses the parameters with respect to the cost of the LBSS operation and establishes appropriate mathematic models for system planning. Section 3 proposes an intelligent algorithm using the Biogeography-Based Optimisation (BBO) approach for the simultaneous storage capacity design and operation strategy formulation of LBSS. Results and discussion for a planning case of a CHP system in the University of Warwick (UoW) are presented in Section 4, before the Conclusion.

## 2. Techno-economic modelling of LBSS

### 2.1. ToU pricing structure

ToU pricing is a rate structure reflecting the cost associated with electricity production throughout the day [16]. In general, ToU tariffs involve high-peak, flat-peak, and low-peak periods. This price difference is the main driver of energy arbitrage by using LBSS. Provided by Western Power-UK, the actual price for purchasing electricity from the grid $C_{elec}$ was composed of the ToU price $C_{ToU}$ and the reactive power charge fee $C_{re}$ shown below in Table 1 and can be represented by

**Table 1**
ToU Electricity price scheme of the grid.

| $C_{ToU}$ High-peak ( $\times 10^{-2}$ GBP/kWh) 16:00 to 19:00 | $C_{ToU}$ Flat-peak ( $\times 10^{-2}$ GBP/kWh) 07:30 to 16:00 19:00 to 21:00 | $C_{ToU}$ Low-peak ( $\times 10^{-2}$ GBP/kWh) 00:00 to 7:30 21:00 to 24:00 | $C_{re}$ Reactive power charge ( $\times 10^{-2}$ GBP/kWh) |
|---|---|---|---|
| 11.301 | 0.433 | 0.048 | 0.393 |

equation (1).

$$C_{elec} = C_{ToU} + C_{re} \tag{1}$$

### 2.2. LBSS operation

#### 2.2.1. Cycle life reduction

The capacity fade caused by anode degradation is the primary reason for the cycle life reduction of LIBs [31]. Typically, there are two kinds of models to evaluate the capacity fade of the battery [27,28,32]. One is the mechanism model which can reach a high precision by studying the electrochemical reaction inside the battery. However, owing to the difficulty in obtaining the precise value of parameters such as conductivity and diffusion coefficient for the apparatus, in addition to the high calculation cost for solving a large number of nonlinear equations, the mechanism model is not suitable for the system-level operation optimisation. The other is the empirical model which could be formulated by the curve fitting using historical experiment data of a certain product. High calculation efficiency of the model could be obtained by avoiding the consideration of complex fade mechanism in this case. To achieve a quick assessment of the cycle life reduction for the evaluation of operation cost, the empirical modelling approach was adopted in this study.

Listed by severity, the operational factors are associated with the cycle life reduction of LIB could be summarised as the working temperature, Depth Of Discharge (DOD), and discharge capacity rate (C-rate) [31,33]. Among them, the working temperature can be regulated to the optimal condition under the function of the air conditioning system, so the latter two factors were taken into account in the current modelling work. According to the previously reported data [34,35], the capacity fade of the battery is proportional to the increase of DOD and discharge C-rate. Taking the $\alpha$ DOD and $\beta$ discharge C-rate as a reference operation condition, the residual cycle life at the time $i+1$ after the $j$th discharge cycle under $\gamma$ C-rate can be represented by the following equation:

$$\begin{aligned} &Cl_{residual}(i+1)|_{\alpha,\beta} = Cl_{residual}(i)|_{\alpha,\beta} - Cl_{loss}(j)|_{\alpha,\beta} \\ &= Cl_{residual}(i)|_{\alpha,\beta} - \frac{Cl_{rated}|_{\alpha,\beta}}{Cl_{rated}|_{\alpha,\gamma}} \frac{SOC(i) - SOC(i+1)}{\alpha} \end{aligned} \tag{2}$$

where $Cl_{residual}$, $Cl_{loss}$ and $Cl_{rated}$ refer to the residual, loss, and rated cycle life of the battery respectively. Then, considering the calendar lifetime of the battery, the daily capital cost of LBSS caused by the cycle life reduction can be represented by the following equation:

$$C_{daily} = C_{invest} \times NOB \times Q_{battery} \times \max\left( \frac{\sum_{j=1}^{n} Cl_{loss}(j)|_{\alpha,\beta}}{Cl_{rated}|_{\alpha,\beta}}, \frac{1}{Lt} \right) \tag{3}$$

where $C_{invest}$ refers to the investment cost per kWh; NOB refers to the Number of Battery; $Q_{battery}$ refers to the capacity of the battery; $n$ refers to the number of the control segment; and $Lt$ refers to the calendar lifetime of the battery. Assuming that the civil works for the batteries have been established, $C_{invest}$ is determined by the capacity scale including the number of batteries and inverters. Based on the empirical data from the battery industry [36], the investment cost per kWh decreases with a rise in capacity, and the descending trend would stabilise when the volume reaches a critical value. In this case, Wright's law can be adopted to establish the investment model of LBSS as follows [37]:

$$C_{invest} = A \times \left( NOB \times Q_{battery} \right)^{B} \tag{4}$$

where $A$ and $B$ refer to the related parameters of the modelling.

#### 2.2.2. Working efficiency

Higher efficiency means less energy loss in the charging or discharging process and could help improve the economy of the LBSS. The efficiency of an LBSS mainly depends on the performance of the battery and inverter. Investigation has shown that the efficiency improves as the C-rate increased and a decrease occurred at a high C-rate level [38]. This trend can be represented by an exponential relationship. On the other hand, the increasing State Of Charge (SOC) would reduce the conversion efficiency of the system because of the electronic losses [39,40]. To simplify the modelling, the linear interpolation approach was used to represent the efficiency of the LBSS at $\gamma$ C-rate and $\theta$ SOC according to the measured value at the upper and lower limit of the SOC:

$$\eta(\gamma,\theta) = \eta|_{\gamma,SOC[lower]} - \frac{\left( \eta|_{\gamma,SOC[lower]} - \eta|_{\gamma,SOC[upper]} \right)(\theta - SOC[lower])}{(SOC[upper] - SOC[lower])} \tag{5}$$

where SOC[lower] and SOC[upper] refer to the lower and upper limit of the SOC. Then, the SOC at the time $i$+1 during the charging and discharging process can be approximately represented by the following equation [41].

$$\begin{cases} \text{Charging: } SOC(i+1) = SOC(i) + \dfrac{P\eta(i)\Delta t}{Q_{battery}} \\ \text{Discharging: } SOC(i+1) = SOC(i) - \dfrac{P\Delta t}{\eta(i)Q_{battery}} \end{cases} \tag{6}$$

where $P$ refers to the active power and $\Delta t$ is the time interval. To guarantee the safety and lifetime of the battery, the SOC should be controlled in a region as

$$SOC[lower] \le SOC \le SOC[upper] \tag{7}$$

In addition, the active power also needs to be limited in a certain range as follows:

$$P[lower] \le P \le P[upper] \tag{8}$$

where $P$[lower] and $P$[upper] refer to the lower and upper limit of the active power.

#### 2.2.3. Standby loss

During the standby process, the stored energy in the battery reduced from the ongoing operation of the inverter and the self-discharge of the battery [38,42]. Among them, the former can be considered as a constant value, while the latter increases with the storing SOC [29]. Although a relatively small change in SOC occurred in the standby behavior, the accumulation of this energy loss would increase the system cost and influence the control strategy making to reduce the duration at a high-level SOC. The linear relationship was used in the current study to model the average SOC reduction rate at $\theta$ SOC during the standby process as follows:

$$SOC_{loss} = a \times \theta + b \tag{9}$$

where $a$ and $b$ refer to the related parameters of the modelling. Then the SOC at the time $i$+1 after $\Delta t$ can be simply described as:

$$SOC(i+1) = SOC(i) - SOC_{loss}(i)\Delta t \tag{10}$$

## 3. Economic optimisation

### 3.1. Optimisation model

Considering the time-varying nonlinearity and uncertainty of the whole system, the operation cycle was divided into certain control segments, and in each segment, the decision variables were set to fixed values. Then the optimisation was converted into a dynamic planning problem. To establish an association between the identification of optimum storage capacity and operation strategy, the scale parameter [NOB] and the energy flow parameters [$P_{CHPS}$, $P_{grid}$, $P_{discharge}$] were set as the decision variables of the LBSS. In this way, the objective function

for the minimum cost of system operation per day can be formulated as follows:

$$\begin{aligned}\min f = C_{\text{daily}} + \sum_{j=1}^{n}[(E_{\text{load}}(j) - E_{\text{CHP}}(j)) + \\ + \text{NOB}\left(P_{\text{grid}}(j)t_{\text{charge}}(j) - P_{\text{discharge}}(j)t_{\text{discharge}}(j)\right)]C_{\text{elec}}(j)\end{aligned} \tag{11}$$

where $E_{\text{load}}$ and $E_{\text{CHP}}$ refer to the electrical load demand and CHP generation output, respectively; $P_{\text{CHPS}}$ and $P_{\text{grid}}$ refer to the charge power input by the CHP system and grid for each battery unit; $P_{\text{discharge}}$ refers to the discharge power output by each battery unit; and $t_{\text{charge}}$ and $t_{\text{discharge}}$ refer to the charge and discharge time respectively.

### 3.2. Optimisation algorithm

The BBO approach [43,44], which is characterised by rapid self-convergence and robustness, is applied to solve the proposed combined optimisation issue. Referring to Table 2, a flag accounting for the working mode of the LBSS was introduced as one additional decision variable. Pre-judgment of the validity of the energy flow variables using the flag contributed to simplifying the establishment of logic processes for LBSS operation in the iteration loop and was beneficial to improve the algorithm efficiency by increasing the diversity of the population and narrowing the searching range of the energy variables. In this case, the solution vector of the system in the operation cycle can be represented as:

$$u = \begin{bmatrix} \text{NOB} & \text{NOB} & \dots & \text{NOB} & \text{NOB} \\ P^1_{\text{CHPS}} & P^2_{\text{CHPS}} & \dots & P^{D-1}_{\text{CHPS}} & P^D_{\text{CHPS}} \\ P^1_{\text{grid}} & P^2_{\text{grid}} & \dots & P^{D-1}_{\text{grid}} & P^D_{\text{grid}} \\ P^1_{\text{discharge}} & P^2_{\text{discharge}} & \dots & P^{D-1}_{\text{discharge}} & P^D_{\text{discharge}} \\ F^1 & F^2 & \dots & F^{D-1} & F^D \end{bmatrix} \tag{12}$$

where $D$ refers to the dimension and $F$ refers to the flag.

Detailed steps of the optimisation procedure are described as follows:

Step 1 Input the parameters related to the cost of the LBSS, ToU price, data of the CHP generation and load demand, and system constraints shown in equations (7) and (8).

Step 2 Initialise the BBO parameters. Including Suitability Index Variable (decision variable), dimension (number of the control segment), population size (number of the solution vector), maximum species count, maximum migration rates, maximum mutation rate, elitism parameter, and generation count limit.

Step 3 Initialise a random set of habitats which represent the solution of the LBSS design and control.

Step 4 Calculate the Habitat Suitability Index (HSI) (objective value) for the control segment $i = 1$ to dimension $D$ according to the main logic processes of the LBSS shown in Fig. 1, and map the HSI to the species count.

For the flag 1, the low-price grid power is allowed to be stored in the LIBs for compensating the user load in the flat-peak and high-peak period. Referring to Fig. 1a, the charge efficiency of the LBSS is obtained first using equation (5) and set to a constant value in the current segment. The maximum available CHP charge time $t_{\text{CHPS}}$[max], and the maximum allowable charge time $t_{\text{charge}}$[max] under the power from the CHP and grid are calculated according to equations (6) and (7) to define the profitable energy for storage and avoid the overcharging of the battery. Then the comparison of the above charge time and the time interval in the control segment $t_s$ is conducted to determine the time length of $P_{\text{CHPS}}$ charge, $P_{\text{grid}}$ charge, and standby in each segment. The parameter $P_{\text{CHP}}$ in the Data Pack *II* which refers to the available power output of the CHP are normally greater than $P_{\text{CHPS}}$.

**Table 2**
Flag for the operation mode of LBSS.

| Flag value | Restriction | Description |
|---|---|---|
| 1 | SOC < SOC[upper] | System charging with the grid power is allowed |
| 2 | *E*CHP < *E*load && SOC > SOC[lower] | System discharging |
| 3 | – | System charging with the grid power is not allowed |

Flag 2 depicts that the LBSS is in the discharging process to cover user demand. As shown in Fig. 1b, the discharge efficiency of the LBSS is determined by equation (5) for calculating the maximum discharge time $t_{\text{discharge}}$[max] to ensure that the SOC remains higher than SOC[lower]. Subsequently, $t_s$ is compared with the $t_{\text{discharge}}$ [max] to learn whether there is a standby process. Finally, equations (2)–(4) are used to obtain the residual cycle life and daily capital cost of the LBSS.

When the conditions of the flag 1 or 2 are not satisfied, the logic process would enter the flag 3 mode where the grid power is not allowed for charging. Indicated by Fig. 1c, the batteries are possibly charged only when there is surplus CHP electricity after compensating for the user's needs. Otherwise, the LBSS remains standby status in the current segment. Based on equations (5)–(7), $t_{\text{CHPS}}$[max] and $t_{\text{charge}}$[max] under the CHP power are calculated and regarded as the indexes to determine the time length of charging and standby.

Step 5 Compute the immigration rate and emigration rate, and implement the probabilistic migration and mutation of non-elite habitat. The random disturbance is introduced to the previous generation's best solutions (not including the flag) to generate new individuals for next iteration aiming at the enhancement of the algorithm optimising ability. Then ensure each solution is legal.

Step 6 Go to *step 4* or stop when the generation count limit is reached.

## 4. Case study

A CHP system serving in a "thermal lead" mode in the UoW was investigated in the present work. The system consisted of 3 CHP plants with a total electric power generation of 4.2 MW and thermal energy production of 5.4 MW [45]. Referring to the power supply network shown in Fig. 2a, the electricity produced by the CHP was supplied to the local network with any remaining demand being imported from the grid. Currently, the university does not have an export licence and cannot be paid for any electricity exported to the grid. According to the historic data, the daily net electrical energy ($=E_{\text{CHP}}$-$E_{\text{load}}$) arrangement for each season in 2016 was depicted in Fig. 2b. To improve the degree of power utilisation and gain profit from the ToU electricity rate shown in Table 1, a demonstration of LBSS was introduced and tested, then the optimal integration solution with the CHP was investigated.

### 4.1. LBSS modelling

As shown in Fig. 3a, the LBSS was composed of lithium-ion batteries, bidirectional inverters, transformers, and a data acquisition platform. The specification parameters of the system are shown as follows: $Q_{\text{battery}} = 35$ kWh, $Lt = 3650$ day, $P_{\text{inverter}}$[upper] = 50 kW, $P$[upper] = 35 kW, $P$[lower] = 1 kW, SOC[lower] = 6%, and SOC[upper] = 95%. Historic test data and experiment results shown in Fig. 3b–f were referred to determine the LBSS model for system planning.

(a) Cycle life: generally, it is considered that the battery is out of service when the remaining capacity is reduced to 80% of rated value [46]. The cycling test data of the battery before the invalidation under various DOD and discharge C-rate is shown in

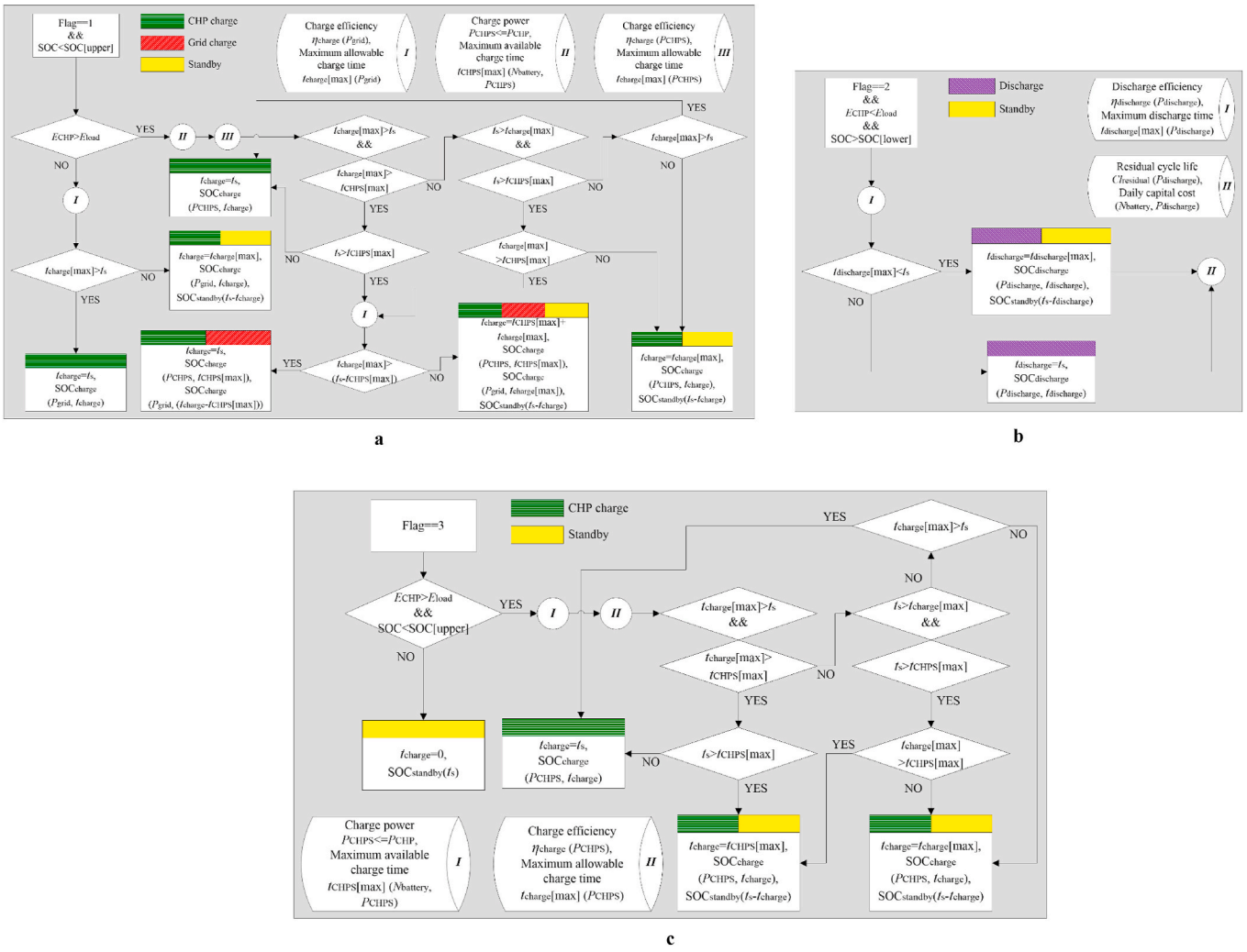


**Fig. 1.** Main logic process of the LBSS operation for combined planning. a, Main logic process of flag 1. **b**, Main logic process of flag 2. **c**, Main logic process of flag 3.

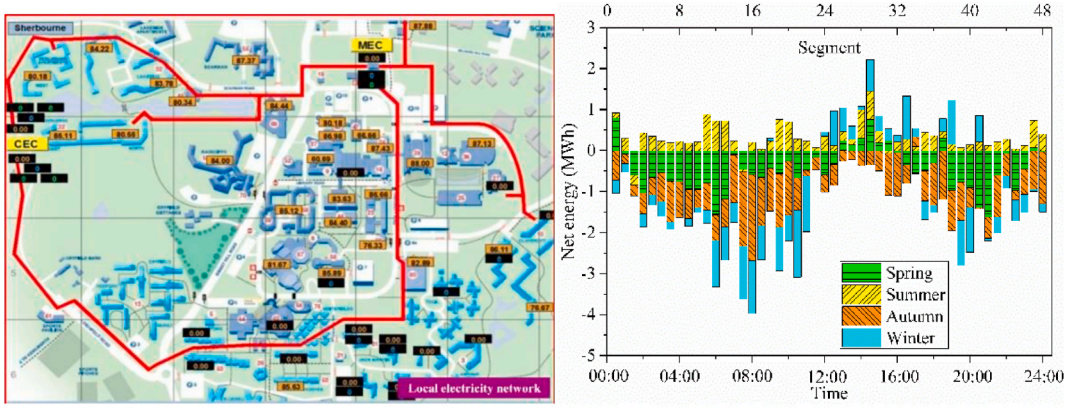


**Fig. 2. Diagram of the power supply network in UoW and the daily net electrical energy of the CHP system for each season in 2016. a**, Power supply network in UoW. **b**, Daily net electrical energy of the CHP system for Spring (April 25), Summer (July 25), Autumn (October 25), and Winter (January 25).

Fig. 3b and c. In detail, when DOD increased from 5% to 90% at 1C discharge rate, the rated cycle life decreased in a linear manner from 120,000 to 6650. On the other hand, lower C-rate led to less reduction in the cycle life: the rated cycle life increased from 6650 to 7075 and 7775 when the C-rate varied from 1C to 0.5C and 0.1C at 90% DOD. Taking the 90% DOD ($\alpha$) and 1 C-rate ($\beta$) as a reference condition, the power law expression can be used to represent the rated cycle life at $\gamma$ C-rate:

$$Cl_{\text{rated}}|_{90\%,\gamma} = (1\text{C}/\gamma)^{0.7} Cl_{\text{rated}}|_{90\%,1\text{C}} \tag{13}$$

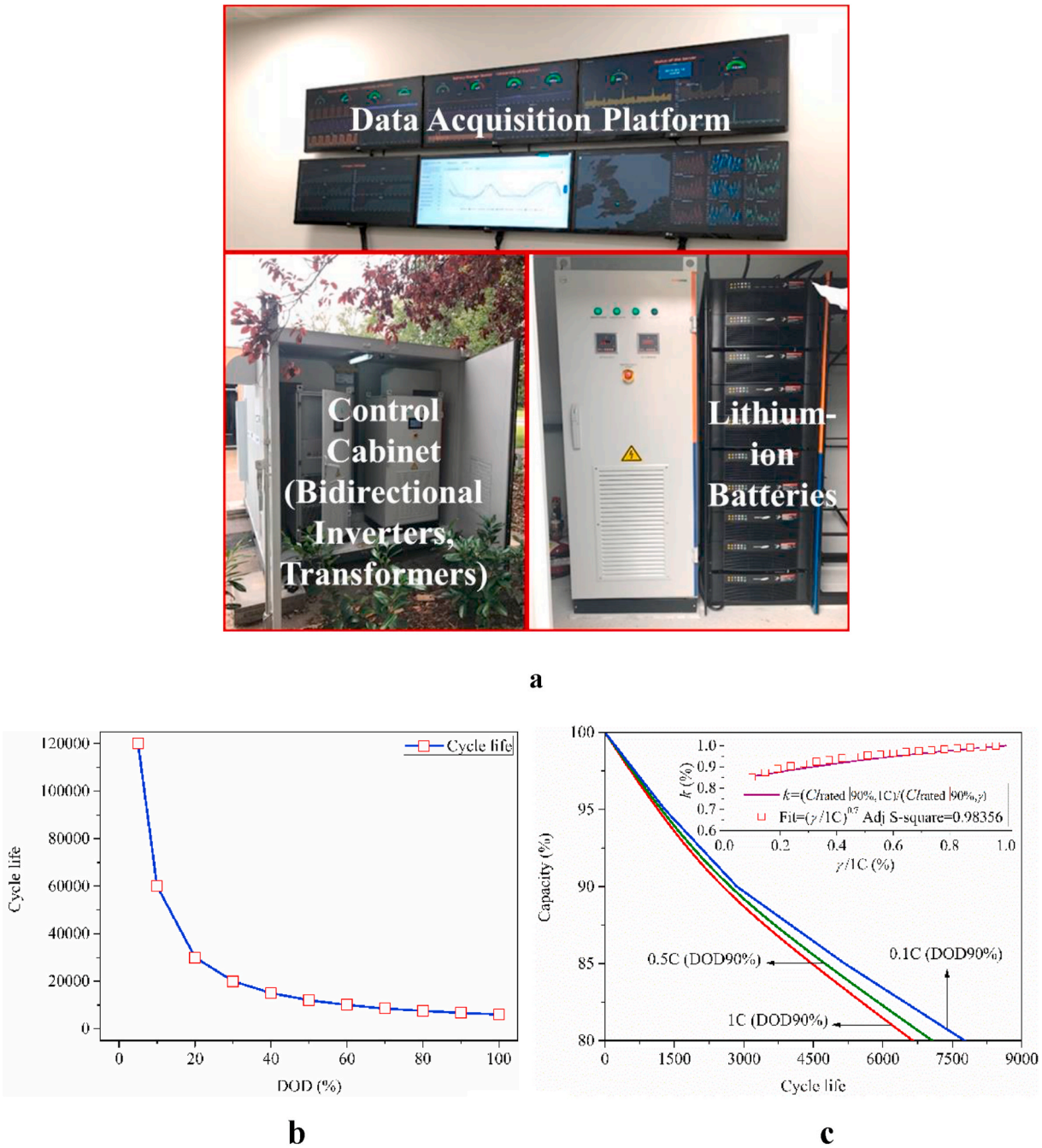


**Fig. 3.** Diagram of the demonstration LBSS and the historic test data and experiment results. a, The demonstration of LBSS. **b**, Cycle life change under various DOD. **c**, Cycle life change under various C-rate. **d**, Investment cost change with capacity **e**, Variation of the charge and discharge efficiency. **f**, SOC loss of the LBSS during the standby process.

According to the provided business data shown in Fig. 3d, the investment cost of the LBSS per kWh decreased with the capacity rising from 300 GBP for a single battery unit and then stabilised at 246 GBP when the total capacity reached 7000 kWh. Curve fitting following Wright's law was implemented according to equation (4) and the parameters associated with the investment cost model were obtained, where $A = 350.5$ and $B = -0.04$. Then the daily capital cost of LBSS can be obtained using equation (3).

(b) Working efficiency: the charge and discharge efficiency of the LBSS at 5%, 50%, and 95% SOC were measured under the inverter power ratio from 5% (2.5 kW) to 100% (50 kW). The trends of the test profiles shown in Fig. 3e were consistent with the description of the work [38–40]. The maximum value of efficiency in the charging and discharging processes can reach 95.53% and 95.94% respectively at 5% SOC and 50% power ratio. The curve fitting analysis following an exponential law was carried out to model the efficiency change with the active power, and the efficiency at $\theta$ SOC can be obtained by the linear interpolation based on the efficiency at 5%, 50%, and 95% SOC.

(c) Standby loss: the SOC reduction of the battery without active power was measured under the SOC lower than 23% and higher than 95%. Referring to Fig. 3f, the average reduction rate in the two cases was 0.19%/h and 0.32%/h respectively. By performing

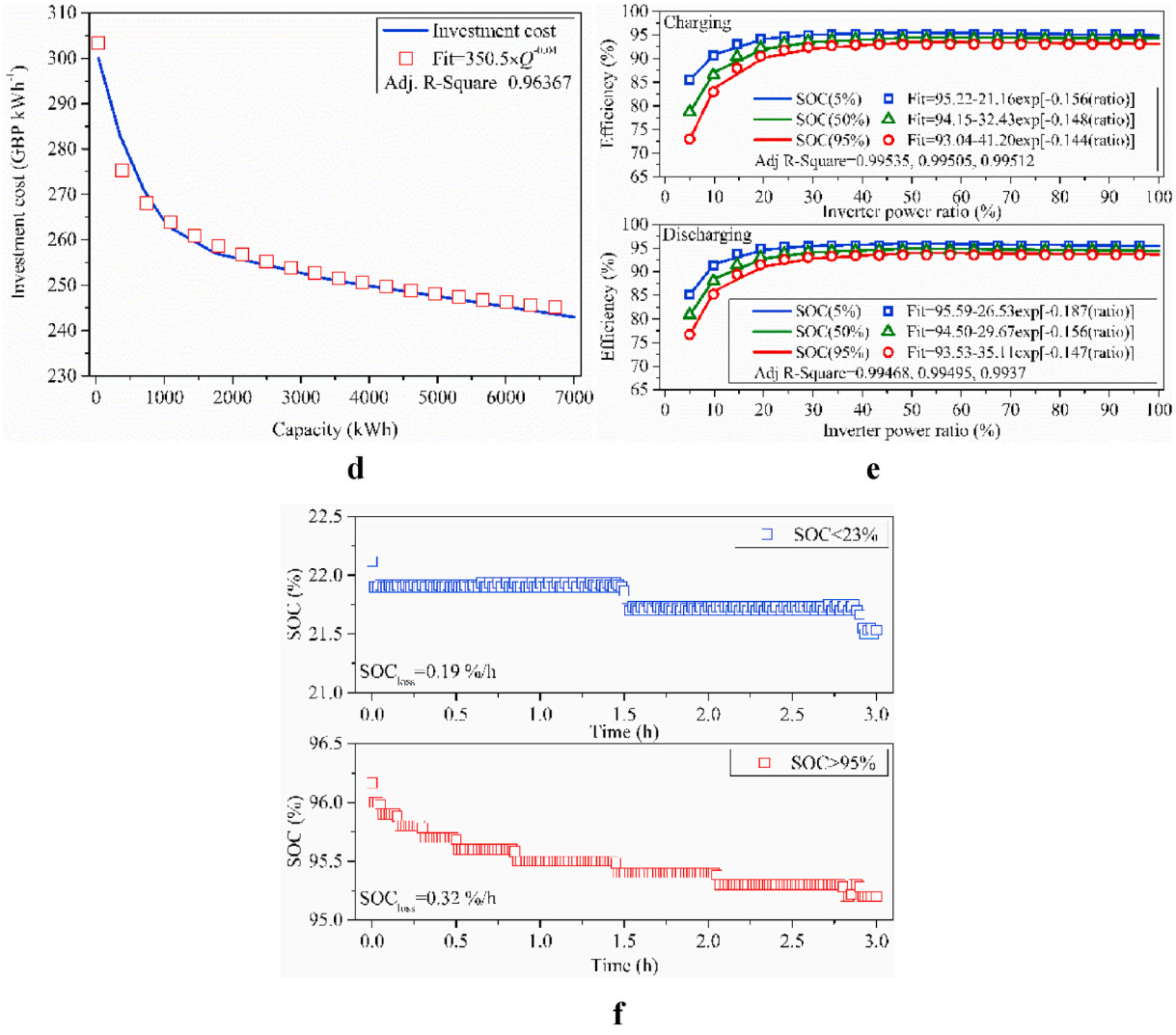


**Fig. 3.** (*continued*).

linear fitting, the model shown in equation (9) can be determined, where $a = 0.18$ and $b = 0.15$.

### 4.2. System optimisation

#### 4.2.1. Seasonal analysis

Seasonal optimisation for the minimum daily cost of the CHP system was carried out and the comparison of the system operation with that under the original CHP system and the common deterministic planning (i.e. battery is charged with the maximum power using the surplus CHP generation power; on the other hand, for the high-peak periods in which a lack of electrical generation exists, the battery is discharged with the maximum power to satisfy the user demand. The capacity of the battery is decided by the minimum value of the surplus energy from the CHP and energy vacancy in the high-peak.) was conducted to verify the effectiveness of the proposed method. Referring to Fig. 2b, a typical day in each season was selected and divided into 48 control segments based on the variation of the load. The optimisation steps discussed in ***Section 3.2*** were conducted to solve the objective function shown in equation (11). The parameters of the BBO were set as follows based on the literature and previous work [43,47]: the population size and generation count limit were 1500 and 2000 respectively, the maximum immigration and emigration rate was 1, the mutation probability was 0.5, the range of the migration probability of each generation was [0, 1], the elitism parameter was 1, and the random disturbance number of optimal solutions was 560.

The analysis results were shown in Fig. 4 and Table 3. Under the combined planning, the net profit of the CHP system can reach £113.7, £0, £142.5, and £15.6 per day, and the corresponding optimum NOB was 82, 0, 141, and 16, respectively. It is worth noting that, for the summer case, the CHP power generation exceeded the user demand during most of the day. Although scattered energy vacancies could be observed, the compensation of the energy gaps by recovering extra CHP power using LBSS was uneconomical compared with purchasing electricity directly from the grid. The one-day payment of electricity in the summer case was £1.94 which was less than the cost of a single LIB unit (= £2.90/day). Therefore, none battery was equipped in this case and the system operation was not affected by the ToU pricing structure.

As shown in Table 3, the combined planning exhibits better economic competitiveness than deterministic planning. The operation strategy of the LBSS for the Spring case shown in Fig. 4b demonstrated that two main operation cycles of the batteries could be observed in combined planning. In the first loop (Segment 1 to 25), the LIBs were fully charged by the residual CHP power and low-peak grid power, then were discharged to 33.2% of SOC for compensating the campus load in the flat-peak. Afterward, the extra CHP power concentrating in Segment 26 to 37 was recovered additionally aiming to fill 98.7% of the electricity gap in the high-peak period. Based on equation (3), the cycle life reduction of the battery caused by the capacity fade was 1.7 (at 1 C-rate, 90% SOC). Through the adjustment of the C-rate, the average efficiency

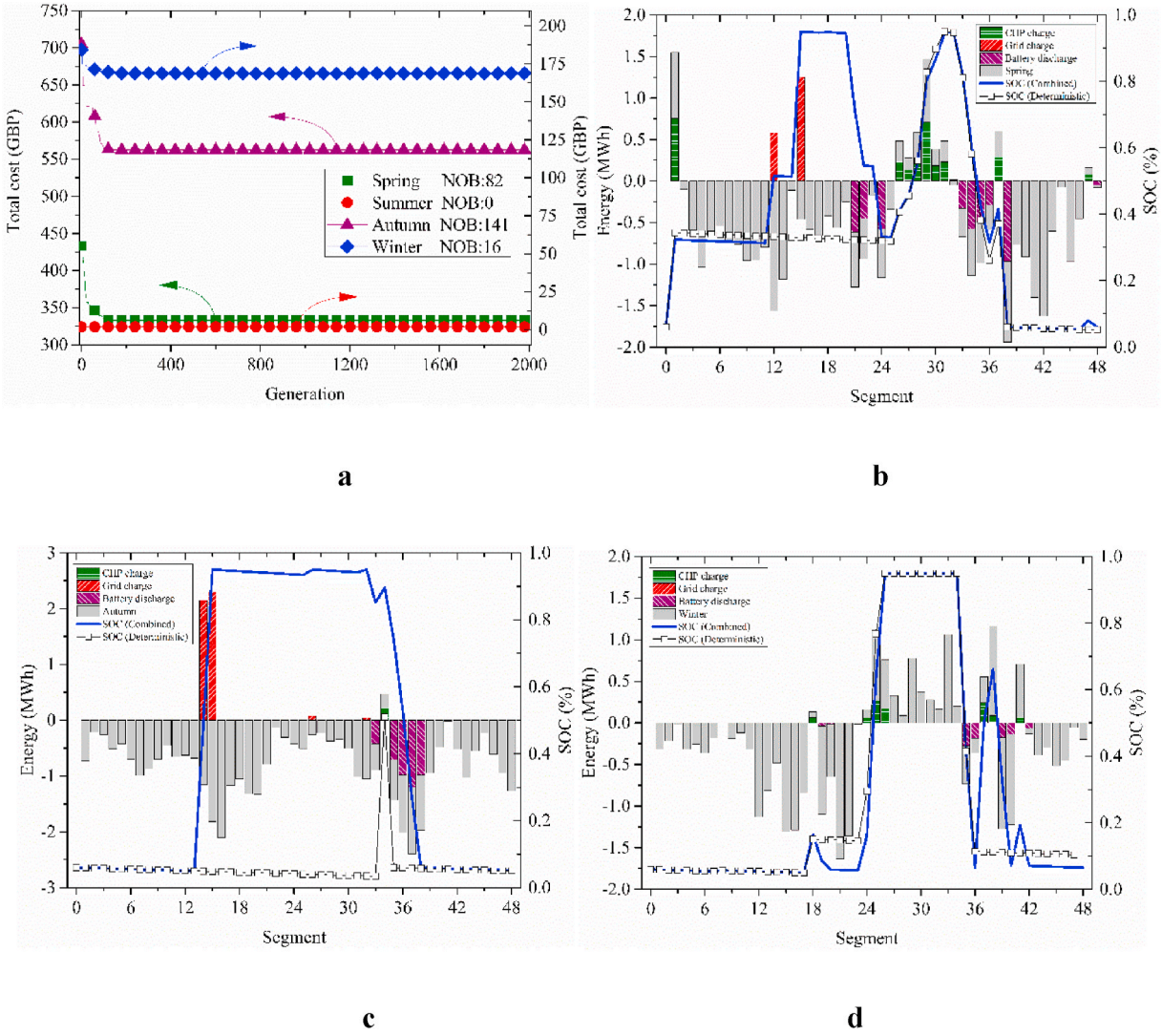


**Fig. 4.** Combined optimisation results for seasons. a, Optimal operation cost and capacity of the LBSS. **b**, Operation strategy of the LBSS for Spring case. **c**, Operation strategy of the LBSS for Autumn case. **d**, Operation strategy of the LBSS for Winter case.

**Table 3**
Comparison of the system operation for each season.

| Season | Case | Grid purchase (£/Day) | NOB | LBSS cost (£/Day) | Net profit (£/Day) |
|---|---|---|---|---|---|
| Spring | Original CHP | 446.4 | – | – | – |
| | Deterministic planning | 155.8 | 76 | 186.3 | 104.3 |
| | Combined planning | 123.5 (user)+8.8 (charge) | 82 | 200.4 | 113.7 |
| Autumn | Original CHP | 705.1 | – | – | – |
| | Deterministic planning | 692.9 | 7 | 18.9 | −6.7 |
| | Combined planning | 203.4 (user)+22.0 (charge) | 141 | 337.2 | 142.5 |
| Winter | Original CHP | 184.3 | – | – | – |
| | Deterministic planning | 126.5 | 18 | 46.7 | 11.1 |
| | Combined planning | 127.0 (user) | 16 | 41.7 | 15.6 |

of the LBSS can reach 94.3% in charging and 91.8% in discharging respectively. The accumulation of the SOC reduction during the standby process was 2.6%, which can result in 75.4 kWh of energy loss in the system. It can be learned that, although smaller LIBs cost occurred in deterministic planning, the absence of the grid power shift from the low-peak to flat-peak and the relatively less energy compensation in the high-peak caused by the ignorance of the actual LBSS efficiency and standby loss yielded more grid purchase cost. In this case, performing combined planning can increase the profit gain of the CHP by 9% compared to the deterministic way.

For the autumn case, because of the shortage of the residual CHP generation, the LIBs were mainly charged by the low-peak grid power and only one cycling of batteries was implemented in combined planning. About 97.5% load in the high-peak zone could be compensated and the total cycle life loss was 1. The average charging efficiency was regulated to 94.2% and the discharging one could reach 92.4%. There was 4.1% of SOC reduction emerged during the standby status where 201.7 kWh total energy loss happened. On the other hand, the integration of LBSS by the deterministic planning resulted in even more capital loss than that in the original system. The reason is that 2.4% of expense reduction in the high-peak (= £ 12.2) by the recovery of the surplus CHP power in segment 35 was smaller than the investment of the storage technology (= £ 18.9). Combined planning reversed this deficit

situation by enlarging storage capacity to make full use of the low-peak power and decreased the payment in the high-peak zone.

Different from the former two cases, in the winter scenario, none grid power participated in the storage process by combined planning because there was abundant residual CHP power can be recovered to gain profit by peak shaving. In this case, the cycle life reduction of the LIB was optimised as 1.82 which was equal to the daily loss calculated using calendar lifetime, and the economics of the system can be improved

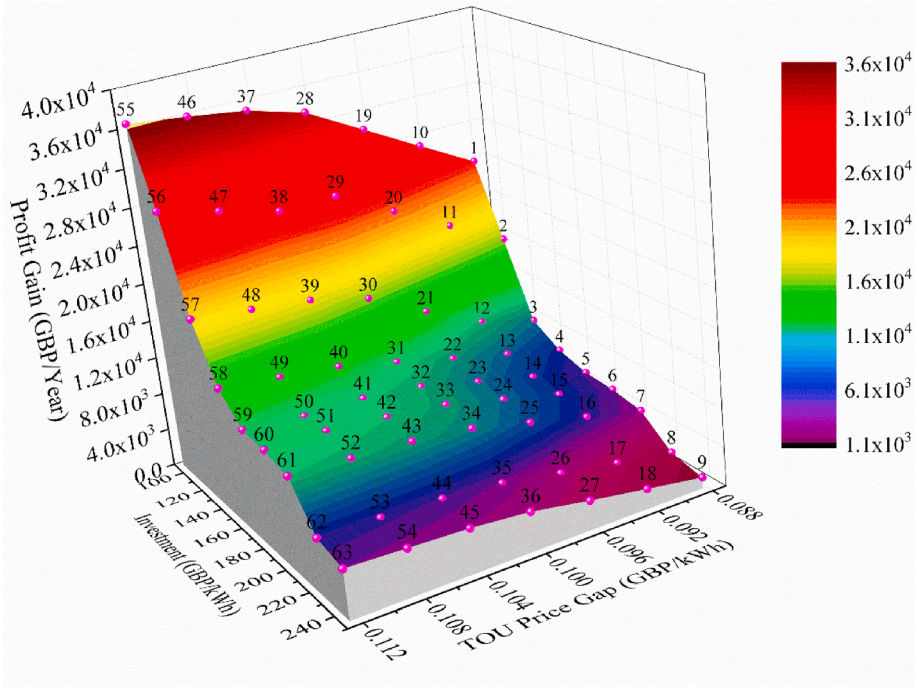


**a**

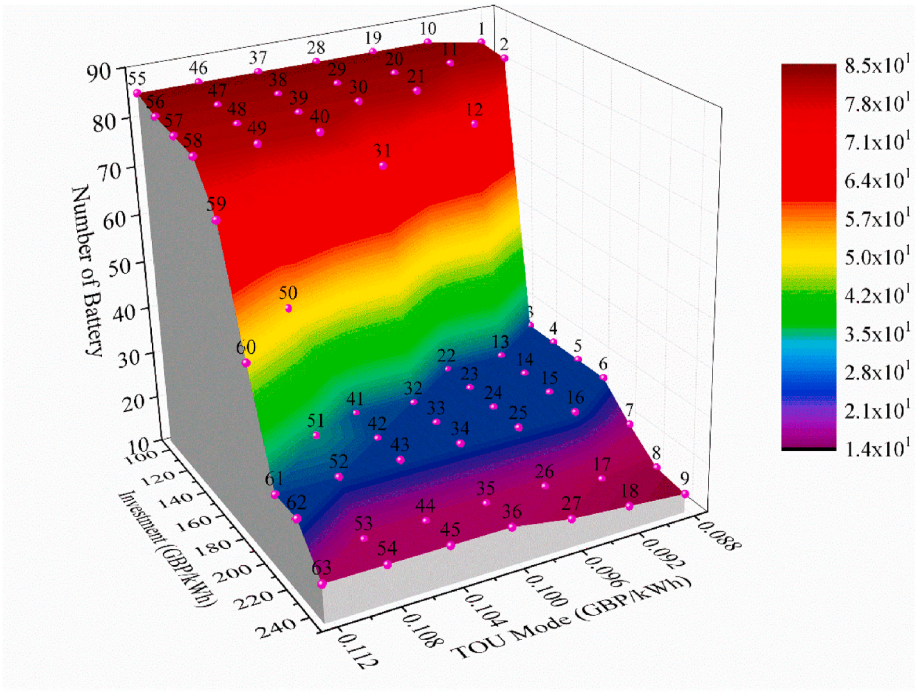


**b**

**Fig. 5.** Combined optimisation results for one year. a, Optimal operation cost with the change of the LBSS price and ToU structure. **b**, Optimal storage capacity with the change of the LBSS price and ToU structure. **c**, Operation strategy of the LBSS for the annual case. **d**, Daily profit with the change of the LBSS price for different seasons. The investment cost of the LBSS decreases from 246 to 92.7 GBP/kWh (7000 kWh-level) and the difference between the high and low-peak electricity price is $11.3 \times 10^{-2}$ GBP/kWh. **e**, Daily profit with the change of the ToU structure for different seasons. The difference between the high and low-peak electricity price narrows from $11.3 \times 10^{-2}$ to $8.8 \times 10^{-2}$ GBP/kWh. The investment cost of the LBSS is 170.7 GBP/kWh (7000 kWh-level).

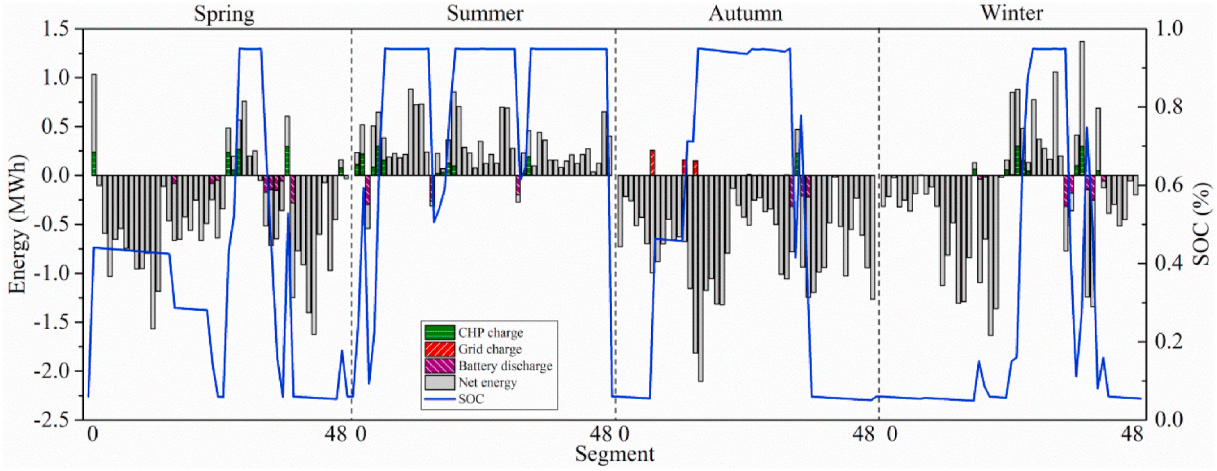


c

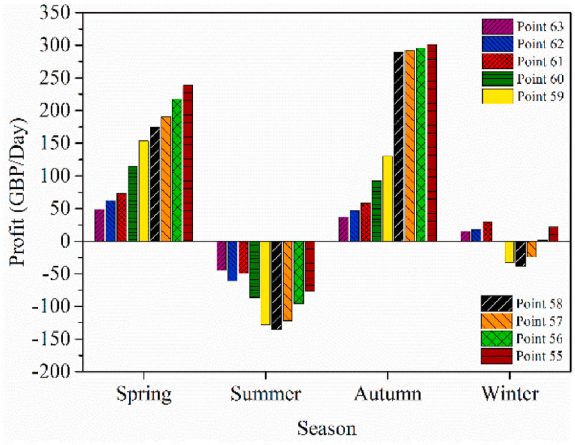


d

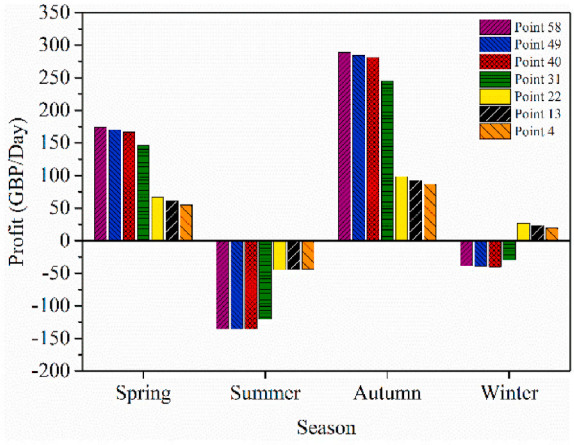


e

**Fig. 5.** (*continued*).

through covering the user load in the high-peak and flat peak (Segment 39 to 42). The average efficiency of charging and discharging can reach 94.2% and 93.6% respectively in this case and the standby SOC reduction for an individual battery was 1.9% which led to 10.4 kWh loss of the whole stored energy. Additionally, it can be learned that still 0.18 MWh of energy shortage remained in the 35th high-peak segment. However, recovering more residual electricity through the enlargement of storage capacity to fill this energy gap would not bring additional cost-saving. The main reason for this situation was the imbalance of the user load of Segment 35 and 36 in the high-peak. The variation cycle of the electricity load was 0.5 h and at least two segments were needed for LIB to get profit from investment under the current ToU rate. However, the load in Segment 35 was 1.5 times larger than that in Segment 36 and the arrangement of battery volume according to this load scale would lead to energy waste in another segment. This viewpoint was verified by the case of using deterministic planning where less grid purchase was achieved while idle battery capacity increased the investment cost and eventually raised the system payment. Under the combined planning, the profit gain of the CHP is 40.5% higher than that obtained by deterministic planning.

#### 4.2.2. Annual analysis

To evaluate the annual profit that can be achieved by the integration of the LBSS, the net energy of the typical days from Spring to Winter is arranged in sequence to represent the distribution of the CHP output and campus load during the whole year. Planning of the LBSS is carried out based on the algorithm shown in Fig. 1. Besides, considering that the price of the LBSS would decrease gradually and the profitability from the ToU structure remains uncertainty in the following decades, this paper investigates the variation trend of profit gain and the corresponding NOB under different LBSS price and ToU rates to predict the future contribution of the LBSS technology in improving the economy of the CHP system [48].

Under the current price of the LBSS and the ToU structure, the economic profit brought to the campus using the LIBs storage can reach 5108.5 GBP/Year (4.2% of the cost for purchasing grid power) and the corresponding NOB is 18 (Point 63 in Fig. 5a and b). The $CO_2$ emission can be reduced by 49.8 ton/Year by using the estimated $CO_2$ emissions over different periods and seasons. (The estimations of $CO_2$ emission were developed using the temporal generation data in 2018 from the grid watch [49] and the generation-based $CO_2$ emissions (ton/MWh) referenced from Refs. [50,51]). The contribution ratio of the recovery of surplus CHP electricity and low-price grid power to the achievement is 5:1. The operation strategy shown in Fig. 5c depicts that, in Spring, the batteries were utilised to mainly recover the additional CHP power in the storage process. According to the storage capacity, the cycle life reduction caused by the discharging process was regulated as that equal to the daily loss calculated using calendar lifetime to make full use of the

battery service. In summer, the surplus CHP energy was transferred by the LIBs to cover the energy gap in the low-peak and flat-peak. However, the profit gain from this action (= £ 1.94/day) was less than the investment cost of the batteries (= £ 47.75/day) and the system operation was under deficit. For the autumn days, the low-peak grid power and the surplus CHP power in Segment 34 were stored to compensate for the campus load in the high-peak. Because of the reduction of the NOB, less profit can be obtained by the peak shaving than that in the single Autumn case. The control strategy for the winter days is similar to that in the single Winter case shown in Fig. 4d and more £ 4.72/day profit from filling the energy gap can be achieved. However, the additional cost of the two more batteries, £ 5.20/day, is less economically competitive than the single Winter planning.

Referring to Fig. 5a and b, for a certain ToU structure, the CHP profits and equipped NOB would increase as the LBSS cost decreases from 246 to 92.7 GBP/kWh (7000 kWh-level) in the next 20 years [48]. For example, under the current electricity price, the annual cost-saving could increase from 5108.5 to 36,542.6 GBP and the correspondent NOB rises from 18 to 85 (Point 63 to 55). It is worth noting that a rapid increase of the NOB can be observed when the investment cost decreases from Point 61 to 58. The reason for this situation is that the reduction of the LBSS cost activates the planning of spring days to the optimal condition shown in the seasonal analysis. Referring to Fig. 5d, from the Point 63 to 61, the cost-saving of the CHP operation is achieved by allowing the economic loss of the LBSS in the summer days and enhancing the profit gain in other seasons. With the further reduction of the LBSS price, the profit pattern of the system turns to cover more energy gap in Spring and Autumn by the enlargement of the storage capacity and sacrifice both the economic gains in the summer and winter days. On the other hand, the economic gains and needed batteries are in the descending trend when the difference between the high and low-peak electricity price narrows from $11.3 \times 10^{-2}$ to $8.8 \times 10^{-2}$ GBP/kWh. Taking the example when the LBSS cost is 170.7 GBP/kWh (Point 58), the profit of the system declined from 13,623.8 to 6363 GBP/Year and the NOB reduced from 81 to 26 (Points 58-49-40-31-22-13-4). It can be learned that an opposite capacity searching process against that in the range of Point 61 to 58 occurred from Point 40 to 22. As shown in Fig. 5e, in the range from Point 58 to 31, the revenue of the system is obtained by maintaining gains in Spring and Autumn using large storage capacity and allowing economic loss in the summer and winter days. After then, the further decrease in the profitability from ToU structure varies the profit pattern of the system and forces a reduction in the storage capacity and increases the economic benefit during the summer and winter days.

## 5. Conclusion

Combined Heat and Power (CHP) systems usually suffer from power mismatch arising from varying electrical demand and uncontrollable power generation in a conventional “thermal-lead” operation. Lithium-ion Battery Storage System (LBSS) could shift energy and improve the power balance between generation and demand and the integrated system would gain economic benefits by using the Time-of-Use (ToU) pricing structures. However, the high-cost, complex control and the relatively quick degradation process of LBSS limit the number of low-carbon applications. To address these issues, a combined planning method was proposed. First, a techno-economic model that describes LBSS-integrated CHP system operation, performance, and economic gains was derived, using the historic and experimental data. Then an integrated optimisation framework with the Biogeography-Based Optimisation (BBO) method that co-optimises battery storage capacity (Capital Expenditure) and temporal operational strategy (Operating Expensed) was proposed, considering control-dependent battery degradation rate at the system planning stage. A real campus-scale CHP system (4.2 MWe and 5.4 MWth) and a 50 kW demonstration LBSS at the University of Warwick (UoW) was used to verify the effectiveness of our proposed method, which also exhibits the contribution of the LBSS in improving the economic performance of CHP systems.

Seasonal application results demonstrated that a combined management mechanism was established to achieve the optimal balance between the profit gain and capital loss of the LBSS integration. The planning solution comprehensively considered the effects of the CHP generation and load distribution, ToU rate, as well as the elements associated with the LBSS operating cost on the system economy. Comparing to the common deterministic planning, the combined planning can increase the profit gain of the CHP system by 9% and 40.5% for the Spring and Winter case respectively and reversed the deficit situation in the autumn days.

The annual planning results showed that, through the combined planning of the capacity design and operation strategy, the LBSS could bring £ 5108.5 of capital revenue per year for the UoW campus which accounted for 4.2% of the total electricity purchasing cost. Meanwhile, the reduction of carbon emission could reach 49.8 tons per year. With a further decrease of the LBSS price (from 246 GBP/kWh to 92.7 GBP/kWh) and potential changes of the ToU structures (the price gap between high-peak and low-peak from $11.3 \times 10^{-2}$ to $8.8 \times 10^{-2}$ GBP/kWh), cost-saving of the CHP system could increase by more than 600% or decrease to 22.4%. The conducted work for maximising potential profits and optimising number of batteries with the change of LBSS cost and ToU structure would provide competitive guidance for investors to develop a reasonable solution to improve the economy of CHP systems by integrating of LBSS in the next decades.

## Credit author statement

**Dacheng Li**: Methodology, Software, Writing – Original Draft. **Songshan Guo**: Investigation, Writing – Review & Editing. **Wei He**: Validation, Writing – Review & Editing. **Marcus King**: Writing – Review & Editing. **Jihong Wang**: Conceptualization, Supervision.

## Declaration of competing interest

The authors declare that they have no known competing financial interests or personal relationships that could have appeared to influence the work reported in this paper.

## Acknowledgements

The authors would like to acknowledge the support of the National Key Research & Development Plan (Grant No. 2017YFB0903601). This work has been conducted as part of the research project ‘Joint UK-India Clean Energy Centre (JUICE)’ which is funded by the RCUK’s Energy Programme (contract no: EP/P003605/1). The projects funders were not directly involved in the writing of this article. The authors would like to acknowledge the support of the West Midlands Regional Energy System Operator (RESO) project (Reference No. 105842). Wei He would like to acknowledge the support of the Royal Academy of Engineering Research Fellowship (Grant No. RF/201819/18/89). Finally, the authors are grateful to Joel Cardinal and Mark Jarvis from Warwick university Estates for giving the access to CHP data server.

## References

[1] Das Barun K, Yasir M, Al-Abdeli. Optimisation of stand-alone hybrid CHP systems meeting electric and heating loads. Energy Convers Manag 2017;153:391–408.
[2] Nouri Alireza, Khodaei Hossein, Darvishan Ayda, Sharifian Seyedmehdi, Ghadimi Noradin. Optimal performance of fuel cell-CHP-battery based micro-grid under real-time energy management: an epsilon constraint method and fuzzy satisfying approach. Energy 2018;159:121–33.
[3] Gvozdenac Dušan, Urošević Branka Gvozdenac, Menke Christoph, Urošević Dragan, Bangviwat Athikom. High efficiency cogeneration: CHP and non-CHP energy. Energy 2017;135:269–78.

[4] Department for Business. Energy & industrial strategy. Combined heat and power. 2018. https://www.gov.uk/guidance/combined-heat-and-power. [Accessed 25 March 2020].
[5] Department for Business, Energy & industrial strategy. Digest of UK energy statistics (DUKES) [Chapter 7]: Combined heat and power 2019.
[6] TechNavio Global Combined heat and power (CHP) market 2019-2023 2019.
[7] Paul Balcombe, Rigby Dan, Azapagic Adisa. Energy self-sufficiency, grid demand variability and consumer costs: integrating solar PV, Stirling engine CHP and battery storage. Appl Energy 2015;155:393–408.
[8] Li Jianwei, Wang Xudong, Zhang Zhenyu, Le Blond Simon, Yang Qingqing, Zhang Min, et al. Analysis of a new design of the hybrid energy storage system used in the residential m-CHP systems. Appl Energy 2017;141:167–79.
[9] Wang Wei, Jing Sitong, Sun Yang, Liu Jizhen, Niu Yuguang, Zeng Deliang, et al. Combined heat and power control considering thermal inertia of district heating network for flexible electric power regulation. Energy 2019;169:988–99.
[10] Haupt Axel, Müller Karsten. Integration of a LOHC storage into a heat-controlled CHP system. Energy 2017;118:1123–30.
[11] Darcovich K, Kenney B, MacNeil DD, Armstrong MM. Control strategies and cycling demands for Li-ion storage batteries in residential micro-cogeneration systems. Appl Energy 2015;141:32–41.
[12] Zhang Chao, Wei Yi-Li, Cao Peng-Fei, Lin Meng-Chang. Energy storage system: current studies on batteries and power condition system. Renew Sustain Energy Rev 2018;82:3091–106.
[13] Sarker Mushfiqur R, Murbach Matthew D, Schwartz Daniel T, Miguel A. Optimal operation of a battery energy storage system: trade-off between grid economics and storage health. Elec Power Syst Res 2017;152:342–9.
[14] Darcovich K, Henquin ER, Kenney B, Davidson IJ, Saldanha N, Beausoleil-Morrison I. Higher-capacity lithium ion battery chemistries for improved residential energy storage with micro-cogeneration. Appl Energy 2013;111:853–61.
[15] Kneiske TM, Braun M, Hidalgo-Rodriguez DI. A new combined control algorithm for PV-CHP hybrid systems. Appl Energy 2018;210:964–73.
[16] Dufo-López Rodolfo, José L, Bernal-Agustín. Techno-economic analysis of grid-connected battery storage. Energy Convers Manag 2015;91:394–404.
[17] Weitzel Timm, Schneider Maximilian, Christoph H, Glock, Löber Florian, Rinderknecht Stephan. Operating a storage-augmented hybrid microgrid considering battery aging costs. J Clean Prod 2018;188:638–54.
[18] Bloomberg. The latest bull case for electric cars: the cheapest batteries ever. 2017. https://www.bloomberg.com/news/articles/2017-12-05/latest-bull-case-for-electric-cars-the-cheapest-batteries-ever. [Accessed 25 March 2020].
[19] Wood Mackenzie, Lacey S. GreenTechMedia – stem CTO: lithium-ion battery prices fell 70% in the last 18 months. https://www.greentechmedia.com/articles/read/stem-cto-weve-seen-battery-prices-fall-70-in-the-last-18-months. [Accessed 25 March 2020].
[20] Hassan Abubakar Sani, Cipcigan Liana, Jenkins Nick. Optimal battery storage operation for PV systems with tariff incentives. Appl Energy 2017;203:422–41.
[21] Arthur Mariaud, Acha Salvador, Ekins-Daukes Ned, Shah Nilay, Markides Christos N. Integrated optimisation of photovoltaic and battery storage systems for UK commercial buildings. Appl Energy 2017;199:466–78.
[22] Kerdphol Thongchart, Fuji Kiyotaka, Mitani Yasunori, Watanabe Masayuki, Qudaih Yaser. Optimization of a battery energy storage system using particle swarm optimization for stand-alone microgrids. Elec Power Syst Res 2016;81:32–9.
[23] Liu Zifa, Chen Yixiao, Zhuo Ranqun, Ji Hongjie. Energy storage capacity optimization for autonomy microgrid considering CHP and EV scheduling. Appl Energy 2018;210:1113–25.
[24] Ranaweera Iromi, Midtgård Ole-Morten. Optimization of operational cost for a grid-supporting PV system with battery storage. Renew Energy 2016;88:262–72.
[25] Wu Xiaohua, Hu Xiaosong, Yin Xiaofeng, Moura Scott J. Stochastic optimal energy management of smart home with PEV energy storage. IEEE Trans Smart Grid 2018;9:2065–75.
[26] Zhang Hao, Cai Jie, Fang Kan, Fu Zhao, Sutherland John W. Operational optimization of a grid-connected factory with onsite photovoltaic and battery storage systems. Appl Energy 2017;205:1538–47.
[27] Ashwin TR, Chung Yongmann M, Wang Jihong. Capacity fade modelling of lithium-ion battery under cyclic loading conditions. J Power Sources 2016;328:586–98.
[28] Liu Yong, Xie Kai, Pan Yi, Wang Hui, Li Yujie, Zheng Chunman. Simplified modeling and parameter estimation to predict calendar life of Li-ion batteries. Solid State Ionics 2018;320:126–31.
[29] Davies DM, Verde MG, Mnyshenko O, Chen YR, Rajeev R, Meng YS, et al. Combined economic and technological evaluation of battery energy storage for grid applications. Nat Energy 2019;4:42–50.
[30] Sarasketa-Zabala E, Gandiaga I, Rodriguez-Martinez LM, Villarreal I. Calendar ageing analysis of a $LiFePO_4$/graphite cell with dynamic model validations: towards realistic lifetime predictions. J Power Sources 2014;272:45–57.
[31] Wang John, Liu Ping, Hicks-Garner Jocelyn, Sherman Elena, Soukiazian Souren, Verbrugge Mark, et al. Cycle-life model for graphite-$LiFePO_4$ cells. J Power Sources 2011;196:3942–8.
[32] Liu Kailong, Kang Li, Ma Haiping, Zhang Jianhua, Qiao Peng. Multi-objective optimization of charging patterns for lithium-ion battery management. Energy Convers Manag 2018;159:151–62.
[33] Hao Menglong, Li Jian, Park Saehong, Scott Moura, Dames Chris. Efficient thermal management of Li-ion batteries with a passive interfacial thermal regulator based on a shape memory alloy. Nat Energy 2018;3:899–906.
[34] Li Jianwei, Gee Anthony M, Zhang Min, Yuan Weijia. Analysis of battery lifetime extension in a SMES-battery hybrid energy storage system using a novel battery lifetime model. Energy 2015;86:175–85.
[35] Ning Gang, Haran Bala, Popov Branko N. Capacity fade study of lithium-ion batteries cycled at high discharge rates. J Power Sources 2003;117:160–9.
[36] Schmidt O, Hawkes A, Gambhir A, Staffell I. The future cost of electrical energy storage based on experience rates. Nat Energy 2017;2:1–8.
[37] Wright TP. Factors affecting the cost of airplanes. J Aeronaut Sci 1936;3:122–8.
[38] Betzin Christopher, Wolfschmidt Holger, Luther Matthias. Electrical operation behavior and energy efficiency of battery systems in a virtual storage power plant for primary control reserve. Elec Power Syst Res 2018;97:138–45.
[39] Ahmadi Leila, Fowler Michael, Young Steven B, Fraser Roydon A, Gaffney Ben, Sean B, Walker. Energy efficiency of Li-ion battery packs re-used in stationary power applications. Sustain Energy Techn 2014;8:9–17.
[40] Michael Schimpe, Naumann Maik, Nam Truong, Holger C, Hesse, Santhanagopalan Shriram, Saxonb Aron, et al. Energy efficiency evaluation of a stationary lithium-ion battery container storage system via electro-thermal modeling and detailed component analysis. Appl Energy 2018;210:211–29.
[41] Ranaweera Iromi, Midtgård Ole-Morten, Korpås Magnus. Distributed control scheme for residential battery energy storage units coupled with PV systems. Renew Energy 2017;113:1099–110.
[42] Grolleau Sébastien, Arnaud Delaille, Gualous Hamid, Gyan Philippe, Renaud Revel, Bernard Julien, et al. On behalf of the SIMCAL Network. Calendar aging of commercial graphite/$LiFePO_4$ cell - predicting capacity fade under time dependent storage conditions. J Power Sources 2014;255:450–8.
[43] Simon D. Biogeography-based optimization. IEEE Trans Evol Comput 2008;6:702–13.
[44] Simon D. A dynamic system model of biogeography-based optimization. Appl Soft Comput 2011;11:5652–61.
[45] Zhao JCC. Thermal energy storage in Warwick campus technique report. UK: University of Warwick; 2010.
[46] Battery technology life verification test manual. INEEL/EXT-04-01986 2005.
[47] Li Dacheng, Wang Jihong, Ding Yulong, Yao Hua, Huang Yun. Dynamic thermal management for industrial waste heat recovery based on phase change material thermal storage. Appl Energy 2019;236:1168–82.
[48] Schmidt Oliver, Melchior Sylvain, Adam Hawkes, Staffell Iain. Projecting the future levelized cost of electricity storage technologies. Joule 2019;3:81–100.
[49] Data courtesy of Elexon portal and Sheffield University. G.B. National grid status. 2018. https://www.gridwatch.templar.co.uk/download.php. [Accessed 25 March 2020].
[50] Grant Wilson IA, Staffell Iain. Rapid fuel switching from coal to natural gas through effective carbon pricing. Nat Energy 2018;3:365–72.
[51] Parliamentary office of Science and Technology. Carbon footprint of electricity generation 2011.